Optimal Design and Control of a Multiscale Model for a Packed Bed Chemical-Looping Combustion Reactor

Kathryn Toffolo*, Luis Ricardez-Sandoval**

**Chemical Engineering Department, University of Waterloo, Waterloo, Canada (Tel: 519-888-4567; email: kmtoffol@uwaterloo.ca).*
*** Chemical Engineering Department, University of Waterloo, Waterloo, Canada (Tel: 519-888-4567x38667; email: laricard@uwaterloo.ca).*

Abstract: Chemical-Looping Combustion (CLC) is a novel carbon capture technology that can be implemented in fossil-fired plants to facilitate the isolation and capture of CO_2. In this work, we present a dynamic multiscale model of this process and implement simultaneous design and control of this reactor in order to investigate its feasibility for industrial use. The model considers both the macroscale reactor behavior and the microscale particle behavior. The optimal design and control formulation is posed as a nonlinear optimization problem that was solved using the direct transcription approach. The optimal solution is compared to that obtained from a sequential design and control approach. The results show that the sequential approach converged to a design that was not able to control the outlet temperature adequately, thus illustrating the benefits of a simultaneous design and control approach.

Keywords: Chemical-looping Combustion, Optimal design and control, CO_2 capture, Economic assessment

1. INTRODUCTION

The atmospheric CO_2 concentration has been increasing ever since the industrial revolution – there has been a rise in CO_2 emmissions which accumulate in the atmosphere and trap heat, driving an increase in the average global temperature known as global warming. In order to cap the global temperature increase and mitigate the worst effects of global warming, there is considerable focus on reducing carbon dioxide emissions (Withey et al., 2020), and new technologies are being investigated to accomplish this goal. CLC is a novel technology used for carbon capture in combustion processes. In CLC, a catalyst is used to avoid contact between the air and fuel streams, preventing unwanted side reactions between the nitrogen naturally present in air and the fuel while facilitating the separation and capture of CO_2 (Lucio and Ricardez-Sandoval, 2020). This effectively combines the combustion and CO_2 separation mechanisms into a single reactor, which employs process intensification (PI). PI is the integration of unit operations in order to improve the efficiency of a process, reduce the cost, and make it more environmentally friendly and sustainable. PI is attracting attention because improved efficiency and reducing the number of units in the process can allow production to occur at lower costs (Charpentier, 2010).

There have been few works examining the dynamic modelling for CLC in a packed bed reactor (PBR) (Han et al., 2013; Noorman et al., 2007). The optimal number and design for CLC PBRs in a power plant was investigated by Spallina et al. (2015); also, there have been studies that investigate optimal control strategies for the CLC processes in a PBR (Han and Bollas, 2016; Lucio and Ricardez-Sandoval, 2020). Studies have been performed on simultaneous optimization of design and control (Burnak et al., 2019); however, to the authors' knowledge, this has not been investigated for packed bed CLC. Sequentially optimizing the design and control for such a system can have lower computational costs, but it does not consider the inherent interactions between design and control, which often results in a more expensive design or less effective operation (Rafiei and Ricardez-Sandoval, 2020). In addition, CLC is a multiscale process, where the macroscale reactor behaviour affects the microscale particle behaviour. Coupled multiscale models are not widely studied because this more complicated system usually entails higher computational costs and complex nonlinear behaviour, but considering interactions between these scales is necessary to accurately capture the system's phenomena (Ricardez-Sandoval, 2011). Despite their growing popularity, optimal design and control has rarely been studied for multiscale systems as the additional interactions make them even more difficult to solve (Rafiei and Ricardez-Sandoval, 2020). However, this could be instrumental in improving the industrial feasibility of CLC by computing the reactor dimensions and control which may reduce costs while maintaining an effective and feasible operation.

In this study, the simultaneous design and control of the oxidation stage for a multiscale packed bed chemical-looping combustion reactor is presented. From this, design and control schemes are obtained which will provide effective operation strategies for this process. Optimizing the design and control of CLC for efficient operation can reduce the cost of energy output by this reactor and make it more economically feasible to implement in gasification power plants, which will reduce the carbon footprint of the process. This work is organized as

follows: in the next section, the CLC process will be briefly described; in the third and fourth section, the model and the formulation for optimal design and control will be presented; in the fifth section, the results will be discussed; concluding remarks and future work are provided at the end.

2. PROCESS DESCRIPTION

CLC is a developing carbon-capture technology in which a metal oxide catalyst is used as an intermediate in the combustion process. This catalyst, usually referred to as an oxygen carrier (OC), is alternatingly exposed to the air and fuel streams. When it is exposed to air, the metal is oxidized as oxygen molecules bind to its surface. This is an exothermic reaction, generating heat which can be sent to a turbine to produce energy. The OC will then be exposed to fuel, reducing and thereby regenerating the oxygen carrier (Han et al., 2013). This process is represented in Fig. 1.

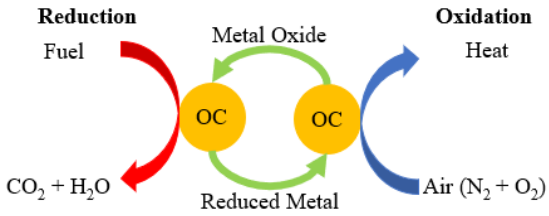

Fig. 1. Schematic representation of the oxygen carrier cycling through the oxidation and reduction stages.

CLC has often been investigated in interconnected fluidized beds; however, looping the catalyst between individual air and fuel reactors requires a separation process to recover the catalyst. Implementing CLC in PBRs is a promising alternative to the fluidized beds. When CLC is performed using a PBR, a single reactor is packed with the OC and alternatingly exposed to air and fuel streams, purging the reactor with an inert gas (e.g. argon) in between these stages. Using a PBR does not require the addition of a separation process and allows the process to operate at higher pressures, increasing the maximum efficiency of the process (Noorman et al., 2007). However, multiple PBRs would be required to maintain a continuous supply of hot air for the turbine.

In this work, the focus will be on the oxidation stage, depicted in Fig. 2. This stage produces heat, and is terminated once the temperature of the outlet gas starts to drop below a user-defined temperature setpoint. However, due to the high amount of energy required for combustion, the OC may not be entirely oxidized by point in time where the process can no longer output gas at the required temperatures (Lucio and Ricardez-Sandoval, 2020). The bulk gas phase models how the temperature and concentration will vary throughout the reactor whereas the OC balance models the diffusion and reaction within the OC particle. The bulk gas and catalyst will interact at the surface of the OC, represented in Fig. 2, and the heat and mass transfer at the catalyst surface must be considered for the reactor balances and for the particle boundary conditions. This is further complicated because the model will be subject to different time and spatial scales within the process. The model for the oxidation stage is presented in the next section.

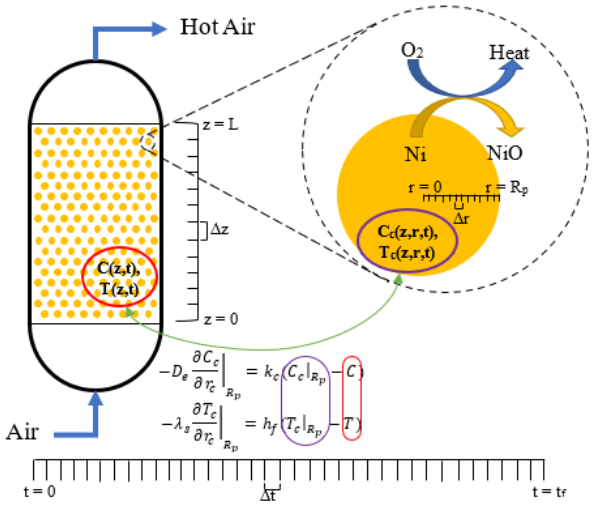

Fig. 2. Schematic representation of the oxidation stage of CLC in a PBR.

3. PACKED BED REACTOR MODEL FORMULATION

The model used to represent the oxidation CLC process in this work is a dynamic model adapted from Han et al. (2013) and Lucio and Ricardez-Sandoval (2020), and was validated using the results reported in Lucio and Ricardez-Sandoval (2020). This model is a multiscale dynamic heterogeneous model, accounting for mass and heat balances within the bulk fluid in the PBR and within the individual oxygen carrier particle. The reactor balance will consider the time and axial position within the reactor, while the particle balances will consider these directions as well as the radial position within the OC particle, as shown in Fig. 2. In this study, nickel oxide supported on alumina is investigated as the OC particle due to its ability to achieve high methane conversion and withstand the high temperatures reached during combustion (Lucio and Ricardez-Sandoval, 2020).

This model is operating under the following assumptions: the OC particles are perfectly spherical, have constant volume and a uniform macroscopic structure unaffected by the reaction, contain a uniform metal oxide distribution, and are uniformly distributed in the PBR; the OC particle and gas within its pores are at the same temperature; the gas thermal conductivity is negligible compared to the OC solid thermal conductivity; the feed stream is perfectly mixed and distributed across the PBR's cross-sectional area; and the mass flowrate at the outlet is the same as it is at the inlet, which is the main variable that can be adjusted for control. The equations representing the oxidation stage for the PBR reactor are as follows:

Reactor mass and energy balances:

$$\varepsilon_b \frac{\partial C}{\partial t} + \frac{\partial F}{\partial V} = \varepsilon_b \frac{\partial}{\partial z}\left(D_{ax} \frac{\partial C}{\partial z}\right) + k_c a_v (C_c|_{R_p} - C) \quad (1)$$

$$\varepsilon_b C_{pf} C_T \frac{\partial T}{\partial t} + C_{pf} F_T \frac{\partial T}{\partial V} = \varepsilon_b \frac{\partial}{\partial z}\left(\lambda_{ax} \frac{\partial T}{\partial z}\right) + h_f a_v (T_c|_{R_p} - T) \quad (2)$$

Reactor boundary conditions:

$$\varepsilon_b D_{ax} \frac{\partial C}{\partial z}\Big|_{z=0} = (F|_{z=0} - y_{feed} F_{in})/A_c \quad (3)$$

$$\varepsilon_b \lambda_{ax} \left.\frac{\partial T}{\partial z}\right|_{z=0} = (T_c|_{z=0} - T_{in}) C_{pf} F_T / A_c \quad (4)$$

$$\left.\frac{\partial C}{\partial z}\right|_{z=L} = \left.\frac{\partial T}{\partial z}\right|_{z=L} = 0 \quad (5)$$

Particle phase mass and energy balances:

$$\varepsilon_c \frac{\partial C_c}{\partial t} = \frac{1}{r_c^2} \frac{\partial}{\partial r_c} \left(D_e r_c^2 \frac{\partial C_c}{\partial r_c} \right) - \rho_s R \quad (6)$$

$$\left((1-\varepsilon_c) \rho_s C_{ps} + \varepsilon_c C_{pc} C_T \right) \frac{\partial T_c}{\partial t} = \frac{\lambda_s}{r_c^2} \frac{\partial}{\partial r_c} \left(r_c^2 \frac{\partial T_c}{\partial r_c} \right) - \Delta H \rho_s R \quad (7)$$

Particle phase boundary conditions:

$$-D_e \left.\frac{\partial C_c}{\partial r_c}\right|_{R_p} = k_c (C_c|_{R_p} - C) \quad (8)$$

$$-\lambda_s \left.\frac{\partial T_c}{\partial r_c}\right|_{R_p} = h_f (T_c|_{R_p} - T) \quad (9)$$

$$\left.\frac{\partial C_c}{\partial r_c}\right|_{r_c=0} = \left.\frac{\partial T_c}{\partial r_c}\right|_{r_c=0} = 0 \quad (10)$$

where the time element is represented by t, the axial direction element is represented by z, the radial direction element is represented by r_c, and V represents the volume element. C, C_c, represent the concentrations of oxygen in the reactor and in the gas within the OC (respectively), and C_T represents the total concentration in the gas phase. Likewise, T and T_c represent the temperature in the reactor and OC, respectively. A_c is the cross-sectional area of the PBR, R_p is the radius of the OC, and L is the reactor length. F is the molar flowrate of oxygen and F_T is the total molar flowrate. C_{pf}, C_{pc}, and C_{ps} represent the heat capacity of the gas in the reactor, the gas in the OC, and the OC itself. ε_b and ε_c are the bed and catalyst porosities, and ρ_s is the OC density. k_c and h_f are the mass and heat transfer coefficients between the bulk fluid phase and the OC whereas D_{ax} and D_e are the axial dispersion and effective diffusion coefficients (respectively) of oxygen. The present model assumes that the diffusion can be modelled using binary effective diffusion coefficients. a_v is the external particle surface area per unit volume, y_{feed} is the mole fraction of oxygen in the feed, λ_s is the thermal conductivity of the OC, λ_{ax} is the axial heat dispersion coefficient, R is the rate of reaction, and ΔH is the heat of the oxidation reaction. Several of these parameters, such as k_c, h_f, and λ_{ax}, are estimated using additional mathematical correlations, which are not shown here for brevity but they can be found elsewhere (Lucio and Ricardez-Sandoval, 2020).

The interactions between the macroscale reactor and microscale OC balance are visible in reactor balances (1) and (2), which consider the mass and heat transfer between the reactor and the particle surface (i.e. $C_c|_{Rp}$ and $T_c|_{Rp}$). In addition, the OC boundary conditions (8) and (9) represent the mass and heat transfer between the reactor (C, T) and the surface of the OC. As such, it is evident that the bulk gas in the reactor is impacted by the particle-scale diffusion and reaction, and vice-versa; hence, these two models must be coupled to accurately capture the overall reactor's phenomena. The reactor balances consider the axial and time directions, but the particle balances must also account for the radial direction within the OC, resulting in different discretization schemes for the two scales.

The oxidation reaction taking place is shown in (R1), and the kinetics for this reaction are shown in (11) (Han et al., 2013).

$$2Ni + O_2 \rightarrow 2NiO \quad (R1)$$

$$R = \frac{a_0}{P^{1.02}} k_{0,O_2} e^{-\frac{E_{a,O_2}}{R_g T_c}} (1-X)^{2/3} C_{O_2} C_{Ni}' \quad (11)$$

P is the reactor pressure, a_0 is the initial specific surface area of the OC, $k_{0,O2}$ is the frequency factor for this oxidation reaction, $E_{a,O2}$ is the activation energy of this reaction, R_g is the universal gas constant, X is the conversion of the OC, and C_{Ni}' is the initial concentration of nickel in the OC. Table 1 summarizes the most relevant parameters. More details about this model as well as the rest of the model parameters can be found elsewhere (Lucio and Ricardez-Sandoval, 2020).

Table 1. Model parameters for CLC oxidation.

Parameter	Value
Reactor inlet temperature	450 °C
Reactor pressure	20 bar
Particle radius	2.5e-3 m
Initial concentration of Ni in the OC	0.21 kg Ni/kg OC
Oxygen carrier density	4480 kg/m^3

4. OPTIMAL DESIGN AND CONTROL

Simultaneous design and control is performed in order to determine the design parameters (i.e. reactor diameter, length, and oxidation time) and control actions (i.e. inlet mass flux of air) that results in the lowest cost of electricity (COE) for the oxidation stage of a plant operating with a packed bed CLC under operational constraints. To simplify the analysis, the control scheme is an optimal open loop control strategy using the inlet mass flux as the manipulated variable. A feedback controller could then be tuned to follow the optimal control actions. The outlet gas supplied to the turbine should not undergo sudden temperature changes, which could damage this unit. As such, fluctuations in the outlet temperature during the oxidation stage can be minimized by manipulating the inlet mass flux of air (manipulated variable) to maintain an outlet air temperature (controlled variable) close to 900°C. Hence, the reactor's outlet temperature was chosen as a controlled variable; also, the setpoint (900°C) was chosen because it is safely within the turbine's operable range of 827-1627°C without surpassing the melting point of the oxygen carrier considered in this study (i.e., NiO). Also, this temperature matches the turbine's inlet temperature reported by Han et al. (2013). The equations that define the objective function for this case study are as follows:

$$C_{reac} = C_1 \left(\frac{S_2}{S_1}\right)^n \left(\frac{i_d (1+i_d)^{n_r}}{(1+i_d)^{n_r}-1}\right) \quad (12)$$

$$C_{OC} = C_s \rho_s L A_c (1-\varepsilon_c)(1-\varepsilon_b) \left(\frac{i_d (1+i_d)^{n_{OC}}}{(1+i_d)^{n_{OC}}-1}\right) \quad (13)$$

$$W_{turb} = \eta_{turb} n_{year} \sum_{k=0}^{n_t} \dot{m}(k\Delta t) \Delta H_{turb} \Delta t \quad (14)$$

$$C_{pen} = P_{elec} \frac{n_{year}}{\eta_{heat}} \sum_{k=0}^{n_t} \dot{m}(k\Delta t) \Delta t (T(k\Delta t) - T_{set})^2 \quad (15)$$

Equation (12) determines the capital cost of the reactor; C_1 is the known cost of a reactor, S_1 and S_2 are the volumes of a

reactor of known cost and the given reactor (respectively), and n is a scaling parameter. Equation (13) calculates the cost of the oxygen carrier based on C_s, the cost of the OC (Zhu et al., 2018), and the total mass of the OC in the reactor. Both (12) and (13) are brought to the equivalent annual cost using an expected lifetime of the reactor (n_r) of 25 years, an OC lifetime (n_{OC}) of 5 years, and a discount rate (i_d) of 0.0795, and brought to 2019 costs by using the Chemical Engineering Plant Cost Index. Equation (14) estimates the energy that would be produced by a turbine based on the enthalpy change ΔH_{turb} assuming a turbine inlet temperature at the setpoint of 900°C and turbine outlet temperature of 450°C (reported by He and Lin (2020)). This equation also takes into account the mass flowrate at different time nodes $\dot{m}(k\Delta t)$, a turbine efficiency η_{turb} of 40%, and annual number of reaction cycles n_{year} (calculated based on the annual operational time and the duration of each cycle, assuming 3,500s per cycle for the reduction and purge stages).

To solve the process model shown in (1)-(11), scaling was implemented in the PDEs for the time and axial directions, i.e. both z and t were set to the domain [0,1]. The PDEs were scaled by the reactor length L and final time t_f, respectively. For instance, the time domain was scaled to a normalized horizon, i.e. $t \in (1/t_f)[0, t_f] = [0,1]$. The final time is defined as $t_f = n_t\Delta t$; where n_t is the number of time nodes and Δt is the length of each time node. Likewise, for the length, $L = n_z\Delta z$, where n_z is the number of nodes in the axial direction. The number of time and spatial nodes (n_t and n_z) were chosen *a priori* such that the system can be adequately represented over the axial and time spans considered in this study. Both t_f and L are optimization variables and are used to re-introduce the magnitude and units of time and length into the PDEs. Accordingly, Equations (14) and (15) are multiplied by t_f, to re-introduce the magnitude and units of the time domain. Moreover, Equation (15) is a penalty function that computes the errors on the difference in energy between the actual temperature of the air at the outlet and the reactor's outlet temperature setpoint (900°C). P_{elec} is the cost of electricity, \$0.106/kWh, and η_{heat} is the heater efficiency, 75%. The formulation to address the optimal design and control of the CLC PBR based on (12)-(15) is as follows:

$$\min_{L,D,t_f,G(k\Delta t)} COE = \frac{C_{reac}+C_{OC}+C_{pen}}{W_{turb}} \quad (16)$$

Subject to:

CLC PBR model: Eq. (1)-(11)

$4.0 \le D \le 5.5$

$3.5 \le L/D \le 4.5$

$2600 \le t_f \le 3400$

$2.0 \le G(k\Delta t) \le 4.5$

Where:

$$t \in \frac{1}{t_f}[0, t_f] = [0,1];\ t_f = n_t\Delta t$$

$$z \in \frac{1}{L}[0, L] = [0,1];\ L = n_z\Delta z$$

This nonlinear optimization formulation aims to find the reactor length L (m), the reactor diameter D (m), the duration of the oxidation stage t_f (s), and the control actions for inlet mass flux at each time node $G(k\Delta t)$ (kg/m^2/s) to ensure efficient operation of the reactor while maintaining a low cost of electricity COE (\$/kWh). COE is the overall cost to produce each kWh of electricity, based on the annual design and operation costs and energy output. The reactor diameter has an upper limit of 5.5 m due to construction constraints (Spallina et al., 2015); likewise, bounds on the reactor's length were set such that they comply with an acceptable L/D ratio.

The partial differential equations (PDEs) shown in Eq. (1)-(11) were discretized using a central finite difference scheme using 34 nodes in time (t), 12 in the axial direction (z), and 12 in the particle's radial direction (r_c). The number of discretization points was determined offline such that the discretization provides acceptable results in reasonable simulation times.

The resulting large-scale (discretized) nonlinear optimization problem was solved using the direct transcription approach. This problem was implemented in Pyomo and solved using the interior point nonlinear optimization algorithm by using the linear solver MA97. While implementing direct transcription and using the discretization scheme described previously, this optimization problem consisted of 81,784 equations and 81,799 variables, and converged to a local optimum with a CPU time just under 600 s with a 2.10 GHz E5-2620 processor.

5. RESULTS AND DISCUSSION

The dynamic optimization problem described in Section 4 converged to a set of design variables shown in Table 2 (Simultaneous Solution). The inlet air mass flux control profile and resulting outlet temperature profile are presented in Fig. 3.

Table 2. Optimal design for a CLC PBR.

Design Variable	Simultaneous Solution	Sequential Solution
Reactor Length (m)	17.96	13.17
Reactor Diameter (m)	5.09	4.79
Oxidation Time (s)	3,189.6	2,600.0

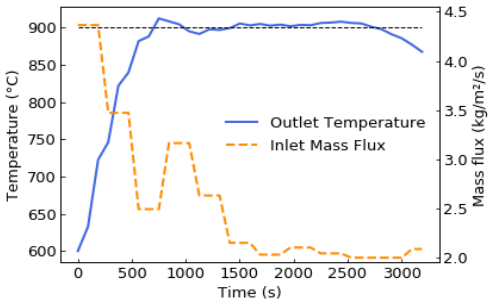

Fig. 3. The optimal mass flux and exit temperature profiles with time for the oxidation stage.

The optimal design of the reactor, shown in Table 2, was quite large despite higher design costs associated with larger

reactors. As shown in Fig. 3, the inlet mass flux is initially quite high, quickly heating up the reactor, and then gradually drops, fluctuating near 2.0 kg/m^2/s for the second half of the oxidation process. The resulting temperature profile requires approximately 600 s to heat up to 900°C, and then fluctuates within about 10°C of the setpoint until it starts to decrease at the end of the oxidation process. As shown in Table 3, the most expensive costs considered in this CLC process are the design costs for the OC and the reactor. The high catalyst cost is expected since it is widely known that Ni-based OCs are very expensive (Zhu et al., 2018). The penalty costs associated with CLC operation are an order of magnitude lower than the design costs, suggesting that the mass flux profile provides appropriate control measures to regulate the outlet temperature. The overall break-even cost of producing electricity when considering these costs would be \$0.131/kWh, without including additional plant-scale costs that should be considered at a larger scale (labour, fuel, etc), which is slightly higher than the \$0.106/kWh average retail COE in the US in 2019 (EIA, 2020). The reported penalty cost is calculated in terms of the enthalpy of air at the reactor outlet.

Table 3. Cost breakdown analysis of the simultaneous scheme

Annualized Expense	Cost
Cost of Reactor, C_{reac} (M\$/yr)	1.29
Cost of OC, C_{OC} (M\$/yr)	2.32
Penalty Costs, C_{pen} (M\$/yr)	0.157
Cost of Electricity, *COE* (\$/kWh)	0.131

In the optimal mass flux profile presented in Fig. 3, there is a peak at 800 s, which does not match the overall mass flux profile at other points in time. The necessity of this peak was further investigated by computing the results for a system with the optimal design but, instead of increasing at 800 s, the mass flux was kept at 2.5 kg/m^2/s from 500 s to 1300 s. Outside of this time frame, the mass flux was kept the same as the optimal solution. Note that the reactor design and oxidation time will be kept the same as those obtained from the optimal solution. Hence, the design and OC costs will not change. As shown in Fig. 4, changing the inlet mass flux results in a considerably different outlet temperature profile which overshoots the setpoint by almost 50°C. Increasing the mass flux increases the rate of reaction, but it also has an even more significant effect on the convection in the system, which may dilute the overall heat being produced. The convective heat transfer term in (2) (i.e. $C_{pf}F_T\frac{\partial T}{\partial V}$) is directly proportional to the flow rate of air entering the system. The air is entering at a lower temperature than the air leaving after the exothermic reaction; thus, higher convection would distribute the energy produced from the reaction amongst a greater quantity of cooler air, thereby decreasing the overall temperature. As such, by increasing the mass flux to 3.3 kg/m^2/s at around 800 s, there will be a less significant increase in the temperature at 1,000 s, resulting in a temperature profile which is kept closer to the setpoint, as predicted by the optimal design and control scheme.

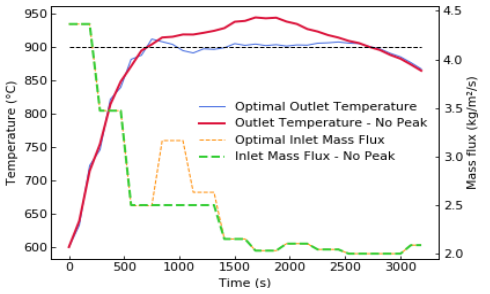

Fig. 4. The comparison of the mass flux and temperature profiles with and without a peak in the mass flux at 800 s.

Fig. 4 shows the importance of finding control profiles through optimization, as the optimal mass flux profile is non-trivial and is adjusted based on the progression of the oxidation reaction. Determining the mass flux profile through the proposed optimization formulation takes the kinetics into account and will exhibit the best control scheme to maintain a consistent temperature profile to effectively operate the plant while protecting the downstream turbine. This change in the inlet mass flux would increase the annual penalty costs by 220% to \$0.501M/yr, increasing the COE by 13.4% to \$0.148/kWh.

To verify whether the optimization formulation for simultaneous design and control is warranted, the design of the CLC PBR using a sequential design and control approach was considered. To perform this task, the inlet mass flux and time were initially held constant at different values (using 2.0 kg/m^2/s and $t_{f,ss}$ = 2600 s resulted in the most optimal reactor design, and only this set of results is shown here for brevity). Under these conditions, the design for the sequential solution (reactor length and diameter) was optimized with respect to the COE for the design, COE_{ss}. This formulation is as follows:

$$\min_{L_{ss},D_{ss}} COE_{ss} = \frac{C_{reac}+C_{OC}+C_{pen}}{W_{turb}} \quad (17)$$

Subject to:

CLC PBR model: Eq. (1)-(11)

$4.0 \le D_{ss} \le 5.5$

$3.5 \le L_{ss}/D_{ss} \le 4.5$

$t_{f,ss}$ = 2600; $G(k\Delta t)$ = 2.0

Where:

$t \in \frac{1}{t_{f,ss}}[0, t_{f,ss}] = [0,1]$, and $t_{f,ss} = n_t \Delta t_{ss}$

$z \in \frac{1}{L,ss}[0, L_{ss}] = [0,1]$, and $L_{ss} = n_z \Delta z_{ss}$

The design parameters obtained from the solution of this problem, L_{ss} and D_{ss}, were fixed to solve for the optimal control profile for this reactor. The formulation to search for the optimal control strategy based on the COE (COE_{SC}) is as follows:

$$\min_{G(k\Delta t),t_f} COE_{sc} = \frac{C_{pen}}{W_{turb}} \quad (18)$$

Subject to:

CLC PBR model: Eq. (1)-(11)

$L=L_{ss}$; $D=D_{ss}$

$2600 \le t_f \le 3400$

$2.0 \leq G(k\Delta t) \leq 4.5$

The resulting optimal design is presented in Table 2 (Sequential Solution); the mass flux and outlet temperature profiles obtained from problem (18) are shown in Fig. 5.

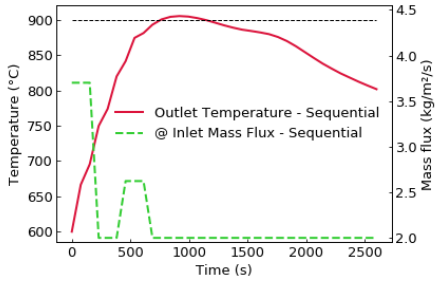

Fig. 5. The mass flux and temperature profiles obtained from sequential optimization of design and control.

The smaller reactor dimensions obtained in the sequential approach reduce the costs of the reactor and OC. However, with such a small reactor, the air is not exposed to enough OC to maintain a temperature at 900°C for an extended period of time. Fig. 5 shows that, even with an optimal mass flux profile, the outlet temperature for this reactor will only briefly reach 900°C before dropping. The design costs were lower than those obtained for the simultaneous design and control scheme ($0.84M/yr for the reactor and $1.51M/yr for the OC). However, the temperature profile for the sequential approach fails to maintain a temperature within the operational range for a gas turbine, resulting in a turbine that may not be operable and therefore would not be able to produce energy, defeating one of the design goals for the CLC process (i.e., produce energy). This is highlighted by the penalties incurred by the outlet temperature's deviation from the setpoint, which were $0.503M/yr (about 3 times larger than the penalties in the simultaneous solution). The overall cost of energy was $0.145/kWh, an 11% increase from the optimal design and control scheme identified in this study.

6. CONCLUSIONS

In this work, a dynamic multiscale model of a packed bed reactor for CLC was used to perform simultaneous optimization of the design and control of this reactor. The problem was formulated using a direct transcription approach. The solution was non-trivial, which highlights the benefits of using optimization to determine the most effective operation strategies. The solution was compared against that obtained from sequential design and control. As expected, sequential optimization resulted in lower design costs, but had higher penalties because the optimal design could not maintain an outlet temperature within the operable range for a gas turbine, meaning that a CLC process would produce very little energy under these conditions. Simultaneous design and control is necessary to consider the transient operation and minimize equipment costs while maintaining efficient operation of the system. Future work in this research will aim to determine how the reduction and purge stages impact the optimal design and operation of the reactor. In addition, an investigation into oxygen carrier selection and packing could be beneficial to determine the most feasible way to implement this novel technology in an industrial-scale power plant.

7. ACKNOWLEDGEMENTS

The financial support provided by the Natural Sciences and Engineering Research Council of Canada (NSERC) is acknowledged.

REFERENCES

Burnak, B., Diangelakis, N. A., and Pistikopoulos, E. N. (2019). Towards the Grand Unification of Process Design, Scheduling, and Control – Utopia or Reality? *Processes*, 7(461).

Charpentier, J.-C. (2010). Among the trends for a modern chemical engineering, the third paradigm: The time and length multiscale approach as an efficient tool for process intensification and product design and engineering. *Chemical Engineering Research and Design,* 88, 248-254.

Energy Information Administration (EIA) (2020). *Average Retail Prices of Electricity.* Retrieved from EIA: https://www.eia.gov/totalenergy/data/monthly/pdf/sec9_11.pdf

Han, L. and Bollas, G. M. (2016). Dynamic optimization of fixed bed chemical-looping combustion processes. *Energy,* 112, 1107-1119.

Han, L., Zhou, Z., and Bollas, G. M. (2013). Heterogeneous modeling of chemical-looping combustion. Part 1: Reactor model. *Chemical Engineering Science,* 104, 233-249.

He, T. and Lin, W. (2020). Energy saving research of natural gas liquefaction plant based on waste heat utilization of gas turbine exhaust. *Energy Conversion and Management,* 225(113468).

Lucio, M. and Ricardez-Sandoval, L. A. (2020). Dynamic modelling and optimal control strategies for chemical-looping combustion. *Fuel,* 262(116544).

Noorman, S., van Sint Annaland, M., and Kuipers, H. (2007). Packed Bed Reactor Technology for Chemical-Looping Combustion. *Industrial & Engineering Chemistry Research,* 46, 4212-4220.

Rafiei, M. and Ricardez-Sandoval, L. A. (2020). New frontiers, challenges, and opportunities in integration of design and control for enterprise-wide sustainability. *Computers and Chemical Engineering,* 132(106610).

Ricardez-Sandoval, L. A. (2011). Current Challenges in the Design and Control of Multiscale Systems. *The Canadian Journal of Chemical Engineering,* 89, 1324-1341.

Spallina, V., Chiesa, P., Martelli, E., Gallucci, F., Romano, M., Lozza, G., and van Sint Annaland, M. (2015). Reactor design and operation strategies for a large-scale packed-bed CLC power plant with coal syngas. *International Journal of Greenhouse Gas Control,* 36, 34-50.

Withey, P., Johnston, C., and Guo, J. (2020). Quantifying the global warming potential of carbon dioxide emissions from bioenergy with carbon capture and storage. *Renewable and Sustainable Energy Reviews,* 115(109408).

Zhu, L., He, Y., Li, L., and Wu, P. (2018). Tech-economic assessment of second-generation CCS: Chemical looping combustion. *Energy,* 144, 915-927.